

Adsorption and self-assembly of aromatic carboxylic acids on Au/electrolyte interfaces

Bo Han · Zhihai Li · Thomas Wandlowski

Received: 20 December 2006 / Revised: 27 January 2007 / Accepted: 30 January 2007 / Published online: 22 February 2007
© Springer-Verlag 2007

Abstract The adsorption and self-assembly of benzoic acid (BA), isophthalic acid (IA), and trimesic acid (TMA) on Au (111) single crystals and on Au(111-25 nm) quasi-single crystalline film electrodes have been investigated in 0.1 M HClO₄ by combining in situ surface-enhanced infrared reflection absorption spectroscopy (SEIRAS) and scanning tunneling microscopy (STM) with cyclic voltammetry. All three acids are physisorbed on the electrode surface in a planar orientation at negative charge densities. Excursion to positive charge densities (or more positive potentials) causes an orientation change from planar to perpendicular. Chemisorbed structures are formed through the coordination of a deprotonated carboxyl group to the positively charged electrode surface. The three acid molecules assemble in different ordered patterns, which are controlled by π -stacking (BA) or intermolecular hydrogen bonds between COOH groups (IA, TMA). A detailed analysis of the potential and time dependencies of the $\nu_{(C=O)}$, $\nu_{s(OCO)}$, and $\nu_{(C-OH)}$ vibration modes shows that the strength of lateral interactions increases upon chemisorption with an increasing number of COOH groups in the sequence of BA<IA<TMA. The vibration bands shift to higher wavenumbers due to dipole–dipole coupling, Stark tuning, and electron back donation from the electrode to COO⁻. In addition, an “indirect” electron donation to the COOH groups takes place via the conjugated molecular skeleton superimposed on the intermolecular hydrogen bonding.

Keywords Aromatic carboxylic acid · Adsorption · Self-assembly · Electrochemistry · SEIRAS · STM

Introduction

Aromatic carboxylic acids, such as benzoic acid (1-benzene-carboxylic acid, BA), isophthalic acid (1,3-benzenedicarboxylic acid, IA), and trimesic acid (1,3,5-benzenetricarboxylic acid, TMA), are composed of a central phenyl ring and peripheral carboxylic groups (COOH). They have been widely used as pattern-controlling units in crystal engineering and supramolecular assemblies such as 1D tapes and ribbons, 2D networks, or 3D bulk crystals [1–4]. These aromatic carboxylic acids and their metal complexes represent prototype building blocks for various molecular nanoarchitectures. Central structure motifs are directional hydrogen bonding and metal ion/ligand coordination [5–14].

Adsorption and self-assembly of several aromatic carboxylic acids and their derivatives were recently studied at electrified solid/liquid interfaces employing electrochemical scanning tunneling microscopy (STM) [15–20]. Here, the electrode potential acts as a universal tuning source to create and to address molecular nanostructures [21, 22].

In situ spectroscopic experiments, especially vibrational spectroscopy, allow one to obtain a direct insight into molecular structures, the interfacial chemical composition, and the interactions within self-assembled adlayers [23, 24]. For example, the adsorption of BA [17, 18, 25, 26], as well as its derivatives such as *p*-nitrobenzoic acid [25], fluoro-benzoic acid [19], and terephthalic acid [20], on Au, Pt, and Ag electrodes were studied by in situ IR methods including infrared reflection absorption spectroscopy (IRAS) and surface-enhanced infrared reflection absorption spectroscopy (SEIRAS). These acids are typically

B. Han · Z. Li · T. Wandlowski (✉)
Institute of Bio- and Nanosystems (IBN-3)
and Center of Nanoelectronic Systems for Information
Technology (CNI), Research Center Jülich,
52425 Jülich, Germany
e-mail: th.wandlowski@fz-juelich.de

physisorbed at negative charge densities (potentials) with the phenyl ring oriented parallel to the electrode surface, and chemisorbed at positive charge densities (potentials) with the ring being tilted or perpendicularly oriented. This structure transition is often accompanied by the deprotonation of at least one of the COOH groups. The analysis of band intensity, peak position, and full width at half maximum (FWHM) reveals the changes in adsorbate–substrate interaction, surface coverage, and long-range order of the adlayer [18, 23, 24].

We have presented a systematic in situ ATR-SEIRAS study on the adsorption of TMA on quasi-single crystalline Au(111–25 nm) film electrodes in our previous work [27, 28]. The steady state chemisorbed adlayer structures were investigated with a specific emphasis on the nature of adsorbate–substrate interactions, the role of intermolecular hydrogen bonding, and the co-adsorption of interfacial water. The SEIRAS results support the coordination of one deprotonated carboxyl group to the positively charged electrode surface in a long-range, ordered “ladder-type” network [27].

The present paper extends our previous experiments to a series of aromatic carboxylic acids having the same conjugated π -electron systems, but different numbers and positions of the COOH groups. We report on a comparative study of BA, IA, and TMA, combining cyclic voltammetric, EC-STM, and in situ SEIRAS investigations. We focus on the influence of the molecular structure, specifically the number and position of the COOH groups, on the molecular adsorption and the self-assembled pattern formation.

Experimental

Electrochemical measurements

The Au(111) electrodes were single crystal cylinders of 4-mm height and 4-mm diameter (EC) or discs of 2-mm height and 10-mm diameter (STM). The gold single crystals were flame-annealed in a butane flame or in a hydrogen flame at red heat (ca. 600 °C), and then cooled in high-purity argon before mounting into the EC or STM cells [28]. The Au samples employed in the spectro-electrochemical ATR-SEIRAS experiments were prepared by electron beam evaporation of thin gold films (25-nm mass thickness) onto the (111)-plane of a highly refractive Si hemisphere, and subsequent electrochemical annealing by cycling the electrode potential in the double layer region in 0.1 M HClO₄ at 50 mV s⁻¹ for ca. 0.5–1 h.

The voltammetric studies were carried out with an AutoLab (PGSTAT-30) or a FHI potentiostat (ELAB-200997). A HEKA (PG-310) potentiostat was employed

to control and synchronize the electrochemical potential during the in situ SEIRAS measurements. The reference electrode (RE) was either a trapped hydrogen electrode (RHE) or a mercury sulfate electrode (MSE). A large-area platinum spiral was used as counter electrode (CE). All potentials in this paper are quoted with respect to a trapped hydrogen electrode (RHE, ca. -310 mV vs. SCE).

ATR-SEIRAS setup

The SEIRAS experiments were carried out employing a vertical spectroelectrochemical cell in a Kretschmann ATR-configuration [23]. The infrared spectra were measured with a Bruker IF66 V/s Fourier transform spectrometer. The spectral resolution was 4 cm⁻¹ in slow-scan and rapid-scan experiments. Non-polarized infrared radiation from a global source was focused onto the electrode–electrolyte interface by passing through the back side of a hemispherical Si prism. The angle of incidence was 70° referring to the surface normal. The spectra are plotted in absorbance units defined as $A = -\log(I/I_0)$ where I and I_0 represent the intensities of the reflected radiation at the actual sample and at the chosen reference potentials, respectively. Further details of the SEIRAS setup and of the spectra acquisition methods were described in our previous publication [23, 27].

Electrochemical STM

The in situ STM experiments were carried out with a Molecular Imaging Pico-SPM using disc-shaped Au(111) single-crystal electrodes. The STM tips were electrochemically etched tungsten tips (0.25-mm diameter), coated with polyethylene. Pt wires served as reference and counter electrodes, respectively. All STM images were recorded in constant current mode with tunneling currents ranging between 3 and 200 pA. More details of the STM setup were provided elsewhere [28].

Chemicals and electrolyte solutions

The solutions were prepared with Milli-Q water (18 M Ω cm, 2–3 ppb TOC), HClO₄ (suprapure, Merck), TMA (for synthesis, Lancaster, twice recrystallized in water), benzoic acid (standard for element analysis, Merck), and isophthalic acid (for synthesis, Merck, twice recrystallized in water).

The glassware was cleaned either in a 1:1 mixture of hot H₂SO₄ and HNO₃, or by soaking in caroic acid, followed by rinsing cycles with Milli-Q water. All electrolytes were deaerated with argon before and during the experiments. The measurements were carried out at room temperature (20±0.5 °C).

Results and discussion

CV and STM

Figure 1 shows a series of typical current vs. potential curves of BA, IA, and TMA on Au(111) in 0.1 M HClO₄. The first voltammetric trace recorded for a carefully prepared unreconstructed Au(111)-(1×1) electrode upon scanning the electrode potential from 0.400 V towards more negative values is represented by the full line. The dashed line shows the steady state cycles, and the dotted trace illustrates the voltammograms of the adsorbate-free supporting electrolyte. The concentrations of the carboxylic acids were chosen between 0.1 and 0.5 of bulk saturation.

One observes two distinct potential regions, II and IV, which are assigned to two-dimensional, long-range ordered physisorbed and chemisorbed adlayers of the respective carboxylic acids [27–29]. The transition is marked by a broad region III. In situ STM experiments reveal that the physisorbed adlayers of BA, IA, and TMA are disordered at $E \leq 0.200$ V (region I) under the experimental conditions chosen in Fig. 1. The corresponding transition I↔II is represented by the decreasing capacitive current for BA and TMA, and a pair of well-developed current peaks P1/P1' in the case of IA. The stability range of II at positive potentials is delimited by a rather broad and asymmetric current peak for BA, and a pair of sharp current peaks P2/P2' for IA. A sequence of high-coverage, physisorbed adlayers of planar-oriented molecules is observed for TMA at the positive edge of region II and in region III [28]. A disordered chemisorbed adlayer is observed at higher potentials, which finally develops into a two-dimensional, long-range, ordered pattern (region IV [28, 29]). Upon reversing the direction of the potential scan, the current peak P3', which is clearly developed for IA and TMA, indicates the dissolution of the ordered chemisorbed adlayer. Multiple cycling smears out the characteristic transition peaks and regions, such as P1/P1', P2/P2', P3/P3', and region III (cf. dashed lines in Fig. 1, [28, 29]).

The insets in Fig. 1 show high-resolution in situ STM images of selected ordered physisorbed and chemisorbed adlayers of BA, IA, and TMA. Flat-lying BA assembles into a square-type pattern of hydrogen-bonded molecules [29]. IA forms hydrogen-bonded zigzag tapes [29, 30]. A hydrogen-bonded honeycomb motif and parallel rows of linear dimers were observed for TMA [28]. These adlayers are stable at an uncharged or slightly negatively charged Au (111)-(1×1) electrode.

The ordered chemisorbed adlayers, which are stable at positively charged gold electrodes, exhibit characteristic assemblies of parallel single (BA) and double striped (IA, TMA) rows. The chemisorbed aromatic carboxylic acids are assumed to assemble with the phenyl group tilted or

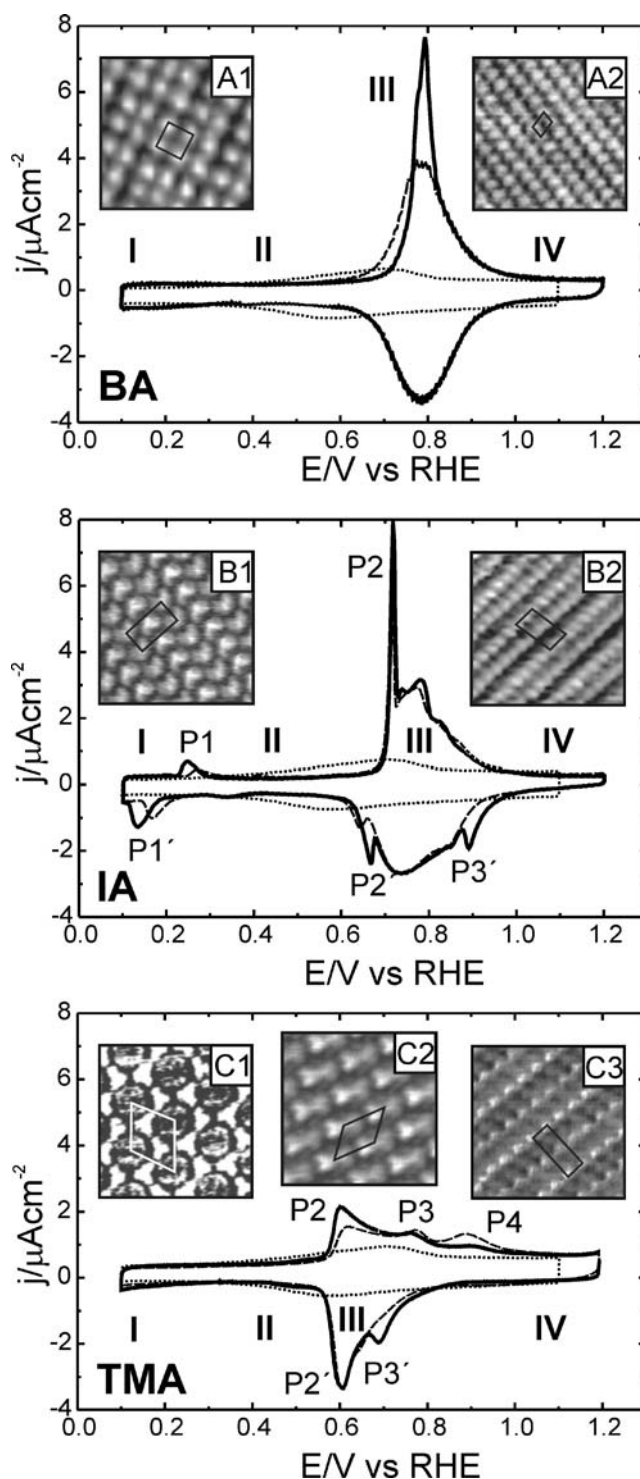


Fig. 1 Cyclic voltammograms (CV) of an ideal Au(111) electrode (miscut angle $< 0.2^\circ$) in 3 mM BA/0.1 M HClO₄, 0.5 mM IA/0.1 M HClO₄, and 3 mM TMA/0.1 M HClO₄ solution, scan rate 10 mV s⁻¹. The *solid lines* represent the first scan recorded after immersion and stabilization at 0.400 V, the *dashed lines* show the steady state cycles, and the *dotted traces* represent the voltammograms in the adsorbate-free supporting electrolyte. The *insets* represent high-resolution in situ STM images of the ordered phases recorded at 0.65 V (A1), 1.20 V (A2; BA, 12 mM), 0.45 V (B1), 1.20 V (B2; IA, 0.5 mM), and 0.30 V (C1), 0.70 V (C2), 1.10 V (C3; TMA, 3 mM), respectively. The scale of all STM images is 5×5 nm

perpendicularly aligned with respect to the surface normal [27].

The suggested repeat motifs of the ordered adlayers are indicated in the high-resolution STM images. The corresponding dimensions and coverages are summarized in Table 1. Clearly, the surface coverage of the physisorbed and chemisorbed adlayers decrease in the following sequence: BA>IA>TMA, which is consistent with the size of the individual molecules. A detailed analysis and discussion of the EC-STM experiments is given elsewhere [28] and [29].

In situ STM experiments and their comparison with crystal structure data reveal clearly that BA, IA, and TMA molecules in the two-dimensional ordered physisorbed state are planar oriented and mutually connected by intermolecular hydrogen bonds between adjacent COOH groups. On the other hand, the STM data do not allow the resolution of the local molecular structure and the coordination in the chemisorbed state. We therefore employed in situ SEIRAS measurements to investigate the structure details in the chemisorbed adlayers.

In situ SEIRAS

Figure 2 shows 3D potential-dependent SEIRA spectra of the BA, IA, and TMA adlayers recorded during a slow potential scan with 10 mV s^{-1} . Characteristic vibration bands are observed at positive potentials in the wavenumber range $1,800 \text{ cm}^{-1} > \nu > 1,200 \text{ cm}^{-1}$, specifically at $1,720$, $1,380$, and $1,300 \text{ cm}^{-1}$. The bands around $1,380 \text{ cm}^{-1}$ are attributed to the symmetric stretching $\nu_s(\text{OCO})$ mode of the COO^- group [31, 32]. Considering the low pH of the electrolyte and the $\text{p}K_a$ values of the three acids (BA: $\text{p}K_a=4.19$; IA: $\text{p}K_a=3.54, 4.60$ [33]; TMA: $\text{p}K_a=2.12, 4.10, \text{ and } 5.18$ [34]), we conclude that the observation of the $\nu_s(\text{OCO})$ bands indicates the chemisorption of molecules onto the gold surface via a COO^- group. The strong vibration bands at $1,720$ (IA), $1,735$ (TMA) cm^{-1} , and the weak bands at $1,290$ (IA) and $1,320$ (TMA) cm^{-1} are

assigned to the stretching modes $\nu_{(\text{C}=\text{O})}$ and $\nu_{(\text{C}-\text{OH})}$ of a protonated COOH group. Comparing to IRAS data and experiments with smooth Au(111) electrodes [17, 18, 25, 26] we roughly estimate an enhancement factor for the symmetric stretching mode $\nu_s(\text{OCO})$ of the three carboxylic acids, which ranges between 10 and 50.

The intensities of all three vibration bands increase during a positive-going potential sweep, and reach their maximum values at $E > 1.000 \text{ V}$. The potential dependencies of the vibration bands of BA and IA support the following scenario referring to the surface selection rule of SEIRAS [35, 36] and the parallel alignment of the vibration dipoles to the phenyl ring: the excursion to positive potentials causes the breakdown of the physisorbed hydrogen-bonded network, and BA and IA molecules change their orientation from planar to tilted or perpendicular accompanied by the deprotonation of at least one of the carboxyl groups. The latter leads to the formation of a substrate–adsorbate coordination complex. A similar sequence was proposed for TMA on gold [27].

Figure 3 shows selected SEIRA spectra at $E=1.1 \text{ V}$ (region IV), which have been recorded simultaneously with a slow scan (10 mV s^{-1}) voltammogram. The correlation analysis of band intensities, as suggested in our previous work [27], demonstrates that each acid is coordinated via only one COO^- group to the positively charged Au substrate. The remaining COOH side groups of IA and TMA, which face the electrolyte, contribute to the formation of an intermolecular hydrogen-bonded network. The intensity ratios between the $\nu_{(\text{C}=\text{O})}$ and the $\nu_{(\text{C}-\text{OH})}$ modes of IA and TMA are similar, indicating that both systems have the side COOH groups with similar orientations in the hydrogen-bonded networks.

Scheme 1 summarizes the structure models of the physisorbed and chemisorbed adlayers of BA, IA, and TMA as derived from the results of the in situ STM and SEIRAS experiments.

Table 1 Details of the STM results for physisorbed (P) and chemisorbed (C) adlayers of BA, IA, and TMA

Molecule	Type of adsorption	Description	Unit cell			Γ ($10^{-10} \text{ mol cm}^{-2}$)
			a (nm)	b (nm)	α ($^\circ$)	
BA (12 mM)	P	Linear dimer	0.79 ± 0.05	0.81 ± 0.05	95 ± 5	2.6 ± 0.3
	C	Single stacking rows	0.58 ± 0.05	0.41 ± 0.05	76 ± 5	7.4 ± 0.2^a
IA (0.5 mM)	P	Zigzag chains	0.74 ± 0.05	1.68 ± 0.05	90 ± 5	2.7 ± 0.3
	C	Double stacking rows	0.80 ± 0.05	1.55 ± 0.05	75 ± 5	5.7 ± 0.3
TMA (3 mM)	PI	Hexagonal honeycomb	1.70 ± 0.08	1.70 ± 0.08	60 ± 6	1.3 ± 0.2
	PII	Linear dimer	1.18 ± 0.05	1.43 ± 0.05	63 ± 5	2.2 ± 0.1
	C	Double stacking rows	0.86 ± 0.05	2.15 ± 0.20	80 ± 5	3.6 ± 0.4

^a The estimated coverage of BA is in good agreement with data recently reported by Li et al. ($7.3 \times 10^{-10} \text{ mol cm}^{-2}$) [18]

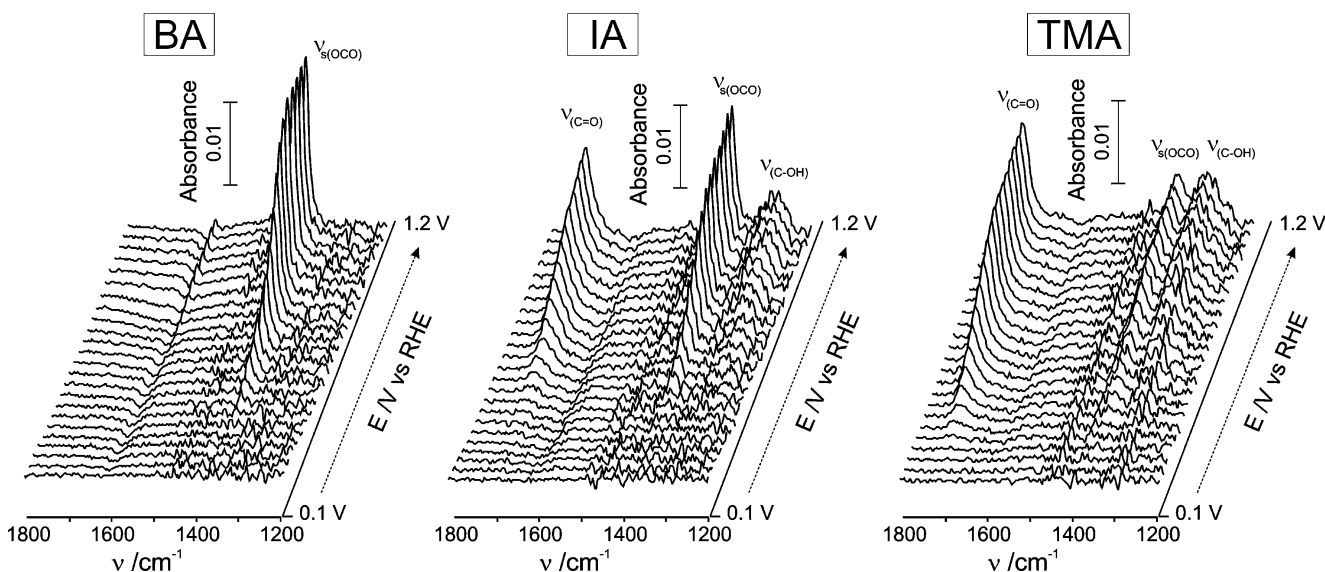


Fig. 2 Typical sets of 3D SEIRA spectra of BA, IA, and TMA adlayers measured simultaneously with the corresponding slow-scan voltammograms (10 mV s^{-1}) during a potential cycle from $E=0.100 \text{ V}$ to $E=1.200 \text{ V}$ and back to $E=0.100 \text{ V}$. For clarity we only show the

spectra recorded during a positive-going potential sweep. The single beam spectrum acquired at $E=0.100 \text{ V}$ is chosen as reference. Each spectrum represents an average of 160 single traces within a potential interval of 50 mV

Interactions within adlayers

In situ SEIRAS provides not only direct structure and chemical information of the adlayers, but also fingerprints

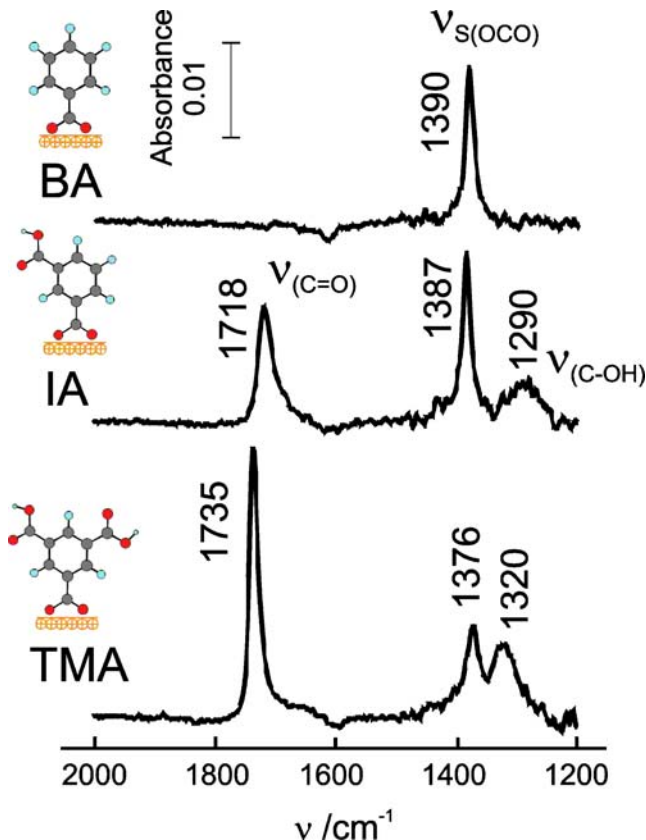
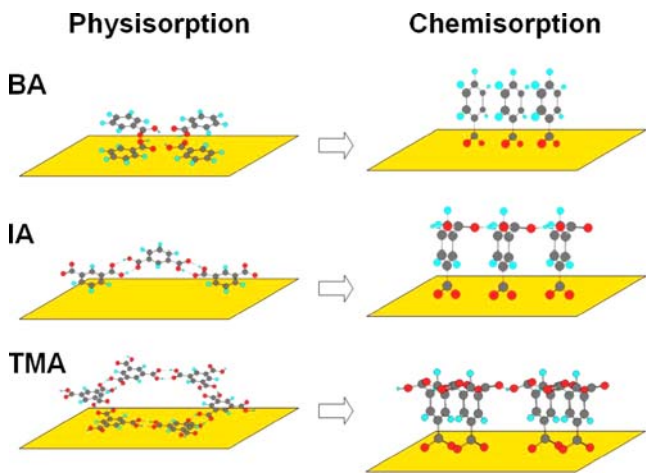


Fig. 3 Selected equilibrium SEIRA spectra of BA, IA, and TMA adlayers obtained at 1.100 V in region IV (chemisorbed phase). The reference spectrum was recorded at $E=0.100 \text{ V}$

of the lateral interactions and of the nature of adsorbate–substrate coupling. This knowledge contributes substantially to the comprehensive understanding of the driving forces for self-assembly. In this contribution we will focus on the IR vibration frequencies of the COOH and COO[−] groups, which are the key functional elements for the lateral hydrogen bonding and the adsorbate–substrate coupling in the chemisorbed adlayer phases (region IV).

As shown in Fig. 3, the maximum frequencies of the $\nu_s(\text{OCO})$ bands decrease in the order BA ($1,390 \text{ cm}^{-1}$)>IA ($1,387 \text{ cm}^{-1}$)>TMA ($1,376 \text{ cm}^{-1}$). This sequence indicates that adsorbate–substrate coupling in the long-range ordered chemisorbed adlayers, which occurs via the COO[−] groups, is weaker with an increasing number of COOH



Scheme 1 Models of the steady-state adlayer structures of BA, IA, and TMA in the potential regions II (physisorption) and IV (chemisorption)

groups. On the other hand, the $\nu_{(\text{C}=\text{O})}$ and $\nu_{(\text{C}-\text{OH})}$ bands of TMA (1,735 and 1,320 cm^{-1}) appear at higher maximum wavenumbers than those of IA (1,718 and 1,290 cm^{-1}), which suggests a stronger lateral interaction via the two hydrogen-bonded COOH groups of each chemisorbed TMA molecule.

The potential (and time) dependencies of the vibration bands provide additional information on the dynamic properties of the transition between the physisorbed and chemisorbed adlayers. The plots of the vibrational frequencies of $\nu_{(\text{C}=\text{O})}$, $\nu_{(\text{C}-\text{OH})}$, and $\nu_{\text{s}(\text{OCO})}$ versus the potential, as obtained from the spectra plotted in Fig. 2, are presented in Fig. 4. Table 2 summarizes the final band positions estimated at $E=1.200$ V and the corresponding peak shifts. Such potential-dependent peak shifts of vibration modes are generally attributed to three different factors: the Stark tuning effect, metal-adsorbate electron (back) donation, and lateral interactions such as π -stacking and dipole–dipole coupling [37–39].

Adsorbate–substrate coupling

The $\nu_{\text{s}(\text{OCO})}$ band of BA shifts to higher frequencies during a positive-going potential sweep. The values of $\nu_{\text{s}(\text{OCO})}$ vs. E increase rather steeply in $0.700 \text{ V} < E < 0.950 \text{ V}$. A linear segment with a considerably smaller slope ($8.47 \text{ cm}^{-1} \text{ V}^{-1}$)

follows at $E > 0.950 \text{ V}$. The steep $\nu_{\text{s}(\text{OCO})}$ vs. E dependence is attributed to an increase of the dipole–dipole coupling upon the orientation change and chemisorption of BA [18]. Peak shifts of similar order of magnitude, which were attributed to a strong dipole–dipole coupling, were observed for close-packed chemisorbed adlayers of several organic molecules, such as cytosine [40], 4,4'-bipyridine [41], BA [15, 18, 19], fumaric acid [42], and uracil [24]. The linear part with a rather small slope in the potential range of chemisorption provides a hint of Stark tuning [18], although there is no strong experimental evidence for a predominant Stark tuning effect, i.e., a uniform linear $\nu_{\text{s}(\text{OCO})}$ vs. E dependence in a large potential range [37]. Compared with the strong dipole–dipole coupling of BA, an electron back donation from the d -levels of the Au electrode into the π^* -orbital of COO^- is less important due to a rather localized π -electron density in the phenyl ring, and a strong σ -bonding between the oxygen and Au atoms [43].

The $\nu_{\text{s}(\text{OCO})}$ band of IA also shifts to higher frequencies during a positive-going potential sweep. However, this blue shift is smaller than that of BA, which is partially attributed to the additional COOH side group. The latter increases the distance between neighboring COO^- groups in the chemisorbed adlayer, and consequently decreases the coupling effect between the dipoles of the COO^- anchors. The hysteresis and the clearly developed plateau in the reversed

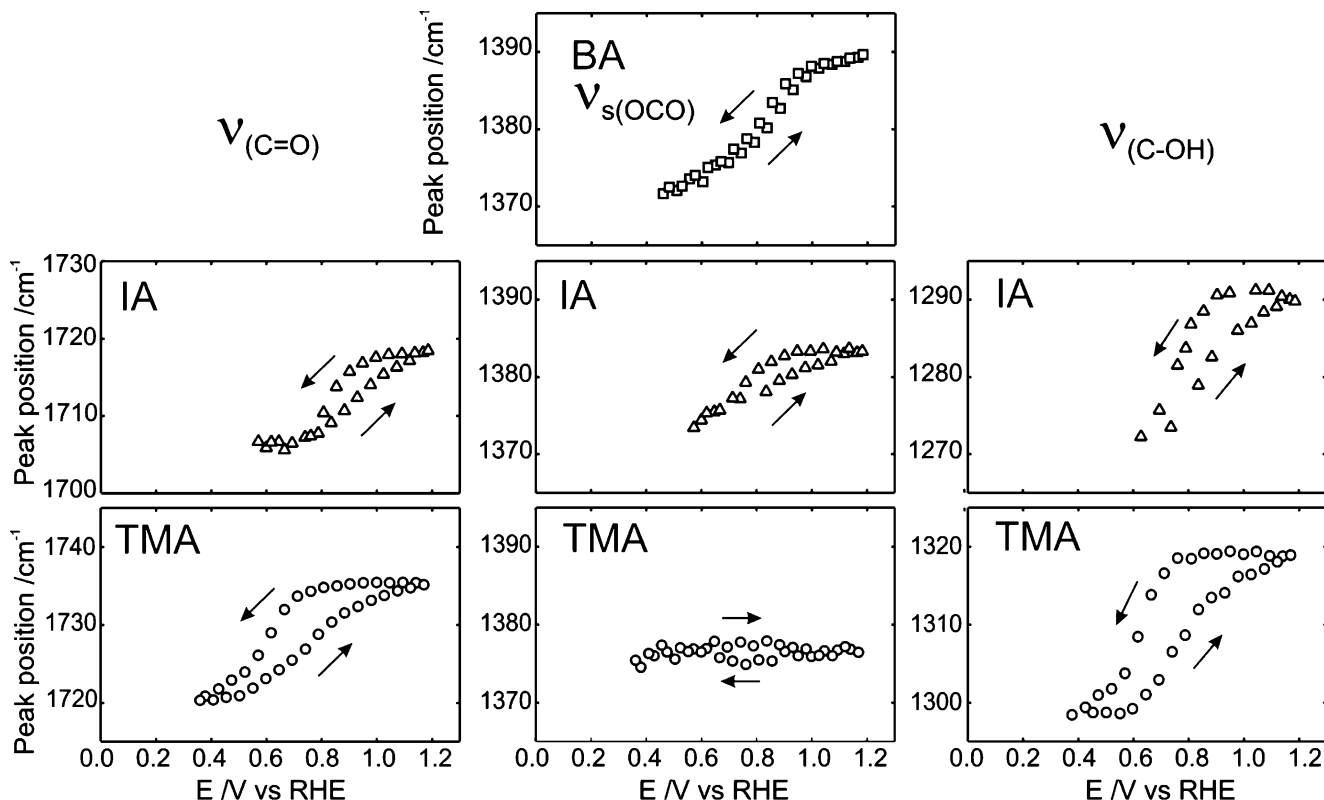


Fig. 4 Potential dependencies of the peak positions of the $\nu_{(\text{C}=\text{O})}$, $\nu_{\text{s}(\text{OCO})}$, and $\nu_{(\text{C}-\text{OH})}$ bands of BA (\square), IA (Δ), and TMA (\circ). The data were extracted from Fig. 2

Table 2 Potential-induced peak shifts (cm^{-1}) of the characteristic COOH and COO^- vibrational modes of different carboxylic acids

	$\nu_{\text{s(OCO)}}$	$\Delta\nu_{\text{s(OCO)}}$	$\nu_{\text{s(C=O)}}$	$\Delta\nu_{\text{s(C=O)}}$	$\nu_{\text{(C-OH)}}$	$\Delta\nu_{\text{(C-OH)}}$
BA	1,390	20	–	–	–	–
IA	1,387	8	1,718	11	1,290	14
TMA	1,376	ca. 0	1,735	15	1,320	20

The $\Delta\nu$ values were obtained from the subtraction of the spectra at 0.40 V (BA, TMA) and 0.60 V (IA) from those at 1.20 V (cf. Fig. 4)

negative-going potential sweep, after the $\nu_{\text{s(OCO)}}$ frequency has reached its maximum at 1.200 V, indicate the formation of a rather stable chemisorbed adlayer of IA.

The slope of the $\nu_{\text{s(OCO)}}$ vs. E plot of TMA is nearly zero. The dipole–dipole coupling within the chemisorbed TMA adlayer is very weak. Neighboring TMA molecules are spatially separated, even further from each other, by two pairs of hydrogen-bonded COOH groups. This explanation is also supported by the STM results, which clearly demonstrate a decreasing packing density in the sequence BA>IA>TMA.

The frequencies of the $\nu_{\text{s(OCO)}}$ mode of IA and TMA are predominantly determined by the Stark tuning effect (blue shift) and the electron back donation (red shift). The dipole–dipole coupling is rather weak. We refer to results of our previous kinetic study in an attempt to distinguish between the two dominant contributions [27]. The establishment of the long-range order within the chemisorbed adlayer due to π -stacking (BA) or hydrogen bonding (IA and TMA) at a fixed potential was tracked by time-resolved SEIRAS in the rapid scan mode. Figure 5 shows the plots of the vibration frequencies $\nu_{\text{(C=O)}}$, $\nu_{\text{(C-OH)}}$, and $\nu_{\text{s(OCO)}}$ as a function of time, recorded after a potential step from region II (physisorption) into region IV (chemisorption). Thus, the constant Stark tuning at fixed potentials can be separated from the overall contribution. The plots of IA and TMA in Fig. 5 show only a red shift for the $\nu_{\text{s(OCO)}}$ mode, which is attributed to electron back donation. As derived from Fig. 4, this red shift is partially (IA) or completely (TMA) compensated by the Stark tuning during a positive-going potential sweep. On the contrary, a blue shift is observed in the time dependence of $\nu_{\text{s(OCO)}}$ for BA, which supports the notions that the compact π -stacking phase of BA (region IV) is dominated by dipole–dipole coupling.

Lateral hydrogen-bonding interaction

The lateral interactions within an adlayer include intermolecular hydrogen bonding and π – π stacking between neighboring phenyl planes. The latter may assist to stabilize the compact packing of chemisorbed BA molecules, but is not predominant for IA and TMA having additional COOH side groups. Therefore, we will focus on the potential dependencies of the $\nu_{\text{(C=O)}}$ and $\nu_{\text{(C-OH)}}$ modes of the COOH groups, which contribute to the formation of an intermolecular hydrogen-bonded ladder network.

As shown in Fig. 4, both bands, $\nu_{\text{(C=O)}}$ and $\nu_{\text{(C-OH)}}$, shift for IA and TMA to higher wavenumbers during a positive-going potential sweep. The most pronounced change occurs also in potential region III, e.g., around the transition between the physisorbed and the chemisorbed state. A plateau develops at positive potentials in the stability region of the chemisorbed phase IV. Upon reversing the direction of the potential scan one observes that the negative edge of the plateau region coincides with P3', the current peak in the voltammograms attributed to the dissolution of the long-range ordered chemisorbed phase. The extension of the plateau region of TMA towards negative potentials (0.400 V) is larger than that of IA (ca. 0.200–0.300 V), indicating a higher stability of the chemisorbed adlayer of the former. The additional COOH group of TMA compared to IA may lead to a more compact hydrogen-bonded network, which supports the perpendicularly aligned TMA molecules in region IV (Scheme 1).

Due to the large distance from the substrate, the frequencies $\nu_{\text{(C=O)}}$ and $\nu_{\text{(C-OH)}}$ are hardly influenced by the strong electric field, which dominates in the immediate vicinity of the electrode [39]. In other words, a strong Stark effect is not very probable. Therefore, the blue shifts of the $\nu_{\text{(C=O)}}$ and $\nu_{\text{(C-OH)}}$ bands are dominantly attributed to intermolecular hydrogen bonding and to an “indirect” electron donation to the COOH side groups via the delocalized π -electron system in the conjugated molecular skeletons of IA and TMA [27, 28]. Similar red shifts due to the delocalization of π -electrons have been predicted and observed for terephthalic acid and conjugated nitriles [20, 44]. The above two factors act simultaneously upon the establishment of the chemisorbed adlayers.

The formation of hydrogen bonds between two COOH groups results often in a red shift of the $\nu_{\text{(C=O)}}$ band, and a blue shift of the $\nu_{\text{(C-OH)}}$ band [45]. However, an electron (back) donation to the COOH side groups may compensate the effect due to hydrogen bonding. In consequence, both bands shift to higher wavenumbers. Similar trends were also observed in kinetic experiments. For example, $\nu_{\text{(C=O)}}$ and $\nu_{\text{(C-OH)}}$ shift to high wavenumbers until their maximum values are reached (ca. 150 s after stepping to the final potential) [27]. Considering the larger $\Delta\nu_{\text{(C=O)}}$ and $\Delta\nu_{\text{(C-OH)}}$ values of TMA compared with IA, we conclude that such an “indirect” electron (back) donation to the COOH moiety appears to be favored by a more stable hydrogen-bonded network.

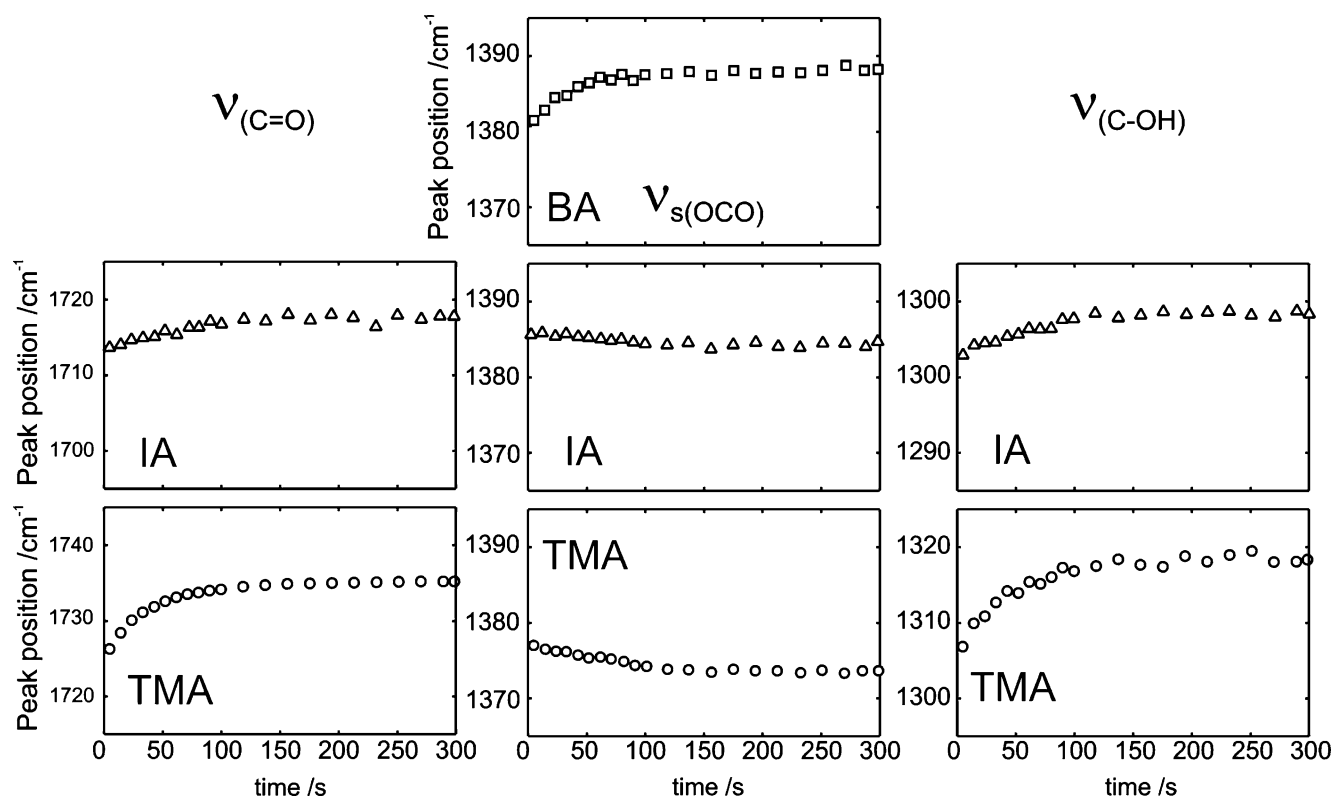


Fig. 5 Time dependencies of the $\nu_{\text{C=O}}$, $\nu_{\text{s(OCO)}}$, and $\nu_{\text{C-OH}}$ bands of BA (\square), IA (Δ), and TMA (\circ) as obtained from time-resolved SEIRA spectra (rapid scan regime [27]) for the formation of chemisorbed adlayers. The data were recorded after a single potential step from $E_i =$

0.450 V to $E_f = 0.900$ V. The waiting time at E_i was 10 s. Each spectrum plotted was acquired in intervals of 9.7 s and represents the average of 256 individual traces

Conclusions

We have investigated the adsorption and self-assembly of BA, IA, and TMA on Au(111)-(1×1) single crystals and Au(111–25 nm) quasi-single crystalline film electrodes in 0.1 M HClO₄ by combining cyclic voltammetry with in situ ATR-SEIRAS and EC STM experiments. The adlayer structure can be tuned by changing the electrode potential. All three acids are physisorbed on the electrode surface in a planar orientation at negative charge densities (regions I and II), and chemisorbed in a tilted or perpendicular orientation at more positive potentials, which correspond to positive charge densities (region IV). Each individual molecule is coordinated onto the surface via one COO[−] group. In both physisorbed and chemisorbed adlayers, the acid molecules are connected to each other via intermolecular hydrogen bonds between adjacent undissociated COOH groups. The adlayers show different structure patterns depending on the change of lateral interactions and the strength of adsorbate–substrate coupling. The structure models and dimensions of the respective unit cells are summarized in Scheme 1 and Table 1.

A detailed analysis of the potential and time dependencies of the carboxyl and of the carboxylate vibration modes

provides a comprehensive understanding of the steady-state structures and dynamic changes as triggered by the electrode potential. The lateral interactions (dipole–dipole coupling, π -stacking, or hydrogen binding) and the adsorbate–substrate coupling (electron (back) donation) determine the structure. They exhibit characteristic potential dependencies. In the chemisorbed adlayers, the strength of lateral interactions increases with an increasing number of COOH groups following the sequence BA < IA < TMA. The adsorbate–substrate coupling is indicated by the electron back donation from the electrode to the COO[−] group and by an indirect electron donation to the COOH side-groups.

The combination of electrochemical methods, in situ STM, and SEIRAS reveals details on the potential-induced assemblies of BA, IA, and TMA monolayers on electrified gold/electrolyte interfaces. The universal role of the electrode potential in tuning the properties of the self-assembled patterns is demonstrated.

Acknowledgements The work was supported by the Volkswagen foundation under grant No. I80–879, IFMIT and the Research Center Jülich. The authors acknowledge the skilful help of U. Linke and of H. J. Bierfeld in preparing the gold single crystals and gold film electrodes.

References

1. Bailey M, Brown CJ (1967) *Acta Crystallogr B* 22:387
2. Alcalá R, Martínez-Carrera S (1972) *Acta Crystallogr B* 25:1671
3. De Feyter S, Gesquiere A, Abdel-Mottaleb MM, Grim PCM, De Schryver FC, Meiners C, Sieffert M, Valiyaveetil S, Müllen K (2000) *Acc Chem Res* 33:520
4. Melendres R, Hamilton AD (1998) *Top Curr Chem* 197:97
5. Barth JV, Costantini G, Kern K (2005) *Nature* 437:671
6. Herbststein FH (1996) In: Atwood JL, MacNico DD, Vögtle DD, Lehn JM (eds) *Comprehensive supramolecular chemistry*, vol 6. Pergamon, New York, pp 61
7. Kolotuchin SV, Thiessen PA, Fenlon EE, Wilson SR, Loweth CJ, Zimmerman SC (1999) *Chem Eur J* 5(9):2537
8. Chatterjee S, Pedireddi VR, Ranganathan A, Rao CNR (2000) *J Mol Structure* 520:107
9. Barth JV, Wechesser J, Lin N, Dmitriev A, Kern K (2003) *Appl Phys A* 76:645
10. Ermer O, Neudörfl J (2001) *Chem Eur J* 7:4961
11. Dai JC, Hu SM, Wu XT, Fu ZY, Du WX, Zhang HH, Sun RQ (2003) *New J Chem* 27:94
12. Melendez RE, Shrama CVK, Zaworotko MJ, Bauer C, Rogers RD (1996) *Angew Chem Int Ed Engl* 35:2213
13. Lin N, Dmitriev A, Weckesser J, Barth JV, Kern K (2002) *Angew Chem Int Ed Engl* 41:4779
14. Messina P, Dmitriev A, Lin N, Spillmann H, Abel M, Barth JV, Kern K (2002) *J Am Chem Soc* 124:14000
15. Ishikawa Y, Ohira A, Sakata M, Hirayama C, Kunitake MJ (2002) *Chem Soc Chem Commun* 2652
16. Su GJ, Zhang HM, Wan LJ, Bai CL, Wandlowski T (2004) *J Phys Chem B* 108:1931
17. Ikezawa Y, Sekiguchi R, Kitazume T (2000) *Electrochim Acta* 46:731
18. Li HQ, Roscoe SG, Lipkowski J (1999) *J Electroanal Chem* 478:67
19. Ikezawa Y, Yoshida A, Sekiguchi R (2000) *Electrochim Acta* 46:769
20. Lee MW, Kim MS, Kim K (1997) *J Mol Struct* 415:93
21. Dretschkow T, Wandlowski T (2003) *Top Appl Phys* 85:259
22. Schultz ZD, Gewirth AA (2005) *Anal Chem* 77:7373
23. Wandlowski T, Ataka K, Pronkin S, Diesing D (2004) *Electrochim Acta* 49:1233
24. Pronkin S, Wandlowski T (2003) *J Electroanal Chem* 550–551:131
25. Li HQ, Roscoe SG, Lipkowski J (2000) *J Solution Chem* 29:987
26. Osawa M, Ikeda M (1991) *J Phys Chem* 95:9914
27. Han B, Li Z, Pronkin S, Wandlowski T (2004) *Can J Chem* 82 (10):1481
28. Li Z, Han B, Wandlowski T (2005) *Langmuir* 21:6915
29. Li Z, Han B, Wandlowski T (2007) (in preparation)
30. de Feyter S, Gesquiere A, Klapper M, Müllen K, Schryver FC (2003) *Nano Lett* 3:1485
31. Arenas JF, Marcos JI (1979) *Spectrochim Acta* 35A:355
32. Gonzalez-Sanchez F (1957) *Spectrochim Acta* 12:17
33. Lide DR (ed) (2001) In: *Handbook of chemistry and physics*, 82nd edn. CRC Press, Boca Raton, pp 8–45
34. Dean JA (1985) In: *Lange's handbook of chemistry*, 13th edn. McGraw-Hill, pp 5–42
35. Osawa M (1997) *Bull Chem Soc Jpn* 70:2861
36. Osawa M (2002) In: Chalmers JM, Griffiths PR (eds) *Handbook of vibrational spectroscopy*, vol 1. Theory and instrumentation. Wiley, Chichester, p 785
37. Nichols R (1992) In: Lipkowski J, Ross PN (eds) *Adsorption of molecules at electrodes*. VCH, New York, p 347
38. Lambert DK (1996) *Electrochim Acta* 41:623
39. Ashley K, Pons S (1988) *Chem Rev* 88:673
40. Ataka K, Osawa M (1999) *J Electroanal Chem* 460:188
41. Wandlowski T, Ataka K, Mayer D (2002) *Langmuir* 18:4331
42. Noda H, Wan LJ, Osawa M (2001) *Phys Chem Chem Phys* 3:3336
43. Kwon YJ, Son DH, Ahn SJ, Kim MS, Kim K (1994) *J Phys Chem* 98:8481
44. Kim SH, Ahn SJ, Kim K (1996) *J Phys Chem* 100:7174
45. Colthup NB, Daley LH, Wiberly SE (1990) *Introduction to infrared and Raman spectroscopy*. Academic Press, Boston